Biophysical Journal, Volume *114*

Supplemental Information

Structural Impact of Phosphorylation and Dielectric Constant Variation on Synaptotagmin's IDR

Michael E. Fealey, Benjamin P. Binder, Vladimir N. Uversky, Anne Hinderliter, and David D. Thomas

Calculation of Compaction Predictor κ

Polyampholytes are a class of intrinsically disordered proteins that have a high frequency of positively and negatively charged amino acids. The Syt 1 IDR falls into this category with ~56% of the amino acids being charged. In the predictive framework developed by Das and Pappu (*1*), a polyampholyte IDP will adopt linear/extended or compact/globular random coils, depending on the distribution of charged side chains in sequence. The physical observable for measurement of compaction in this model is radius of gyration R_g, which is correlated with a computable predictive parameter called κ. The κ term depends on two main terms: σ, the overall charge asymmetry, and σ_i, the local charge asymmetry within a "blob" of linear sequence (usually 5 or 6 residues). How κ was calculated and used to predict the possible compactness of the Syt 1 IDR is shown below (Table S1 and Table S2). The fraction of positive (*f*+) and negative (*f*-) within each 5 or 6 residue *i*-th blob was used to determine σ_i:

$$\sigma_i = (f_+ - f_-)_i^2/(f_+ + f_-)_i \quad \text{Eq. 1}$$

Each blob's charge asymmetry was compared to the IDR's overall charge asymmetry (Eq. 2) to determine the squared deviation (δ) using Eq. 3:

$$\sigma = (f_+ - f_-)^2/(f_+ + f_-) \quad \text{Eq. 2}$$

$$\delta = \sum_{i=1}^{Nblob} (\sigma_i - \sigma)^2/Nblob \quad \text{Eq. 3}$$

Where N_{blob} is the number of blobs in the IDR sequence. Next, δ was determined for a rearranged primary sequence of the IDR amino acids that represents the maximum possible charge segregation. This value (δ_{max} = 0.503) was then used to calculate κ, the parameter used to predict degree of compaction based on Figure 2 from (*1*):

$$\kappa = (\delta/\delta_{max}) \quad \text{Eq. 4}$$

IDR peptide binding to LUVs

To test if the IDR core region bound LUVs whose lipid composition mimicked that of a synaptic vesicle, we prepared liposomes using our previously developed lipid cocktail (*2*, *3*). This lipid composition was designed to mimic the outer leaflet of a synaptic vesicle organelle: 1-stearoyl-2-oleoyl-*sn*-glycero-3-phosphoethanolamine (18:0-18:1 PE); 1-palmitoyl-2-oleoyl-*sn*-glycero-3-phosphoethanolamine (16:0-18:1 PE); 1-stearoyl-2-docosahexaenoyl-*sn*-glycero-3-phosphoethanolamine (18:0-22:6 PE); 1-stearoyl-2-docosahexaenoyl-*sn*-glycero-3-phosphoserine (18:0-22:6 PS); 1-stearoyl-2-oleoyl-*sn*-glycero-3-phosphoserine (18:0-18:1 PS); 1-stearoyl-2-arachidonoyl-*sn*-glycero-3-phospho-(1'-myo-inositol-4',5'-bisphosphate) (18:0-20:4 PI(4,5)P2); 1,2-dioleoyl-*sn*-glycero-3-phospho-(1'-myo-inositol-4',5'-bisphosphate) (18:1-18:1 PI(4,5)P2); 1-palmitoyl-2-oleoyl-*sn*-glycero-3-phosphoinositol (16:0-18:1 PI); cholesterol. For further details preparation, see supporting references 2 and 3.

Co-sedimentation with synaptic vesicle mimic LUVs were performed by incubating 15 μM of either the full-length IDR (a synthetic peptide corresponding to residues 80-156) or the IDR core with part of the acidic C-terminus (residues 97-130) with LUVs for 30 minutes at 22 °C. The concentration of LUVs for each sample ranged from 0-6 mM and total sample volume was 60 μL. After incubation, samples were subsequently spun down in a TLA 100 rotor for 1 hour at 22 °C to pellet LUVs and bound peptide. Depletion of peptide from the resultant

supernatants was then used to assess membrane binding, where 20 μL aliquots were taken from the supernatants and run on SDS-PAGE (Fig. S6).

Nonlinear fitting to two-state folding model

To determine the free energy of folding, we fit CD signal change to a two-state folding model. In a two-state model, there is equilibrium between unfolded (U) and folded (F) states of the protein:

$$K_{eq} = [U]/[F] \quad \text{Eq. 5}$$

The equilibrium constant is directly related to free energy through the Gibbs equation (Eq. 6):

$$\Delta G = -RT\ln(K_{eq}) \quad \text{Eq. 6}$$

In cases where protein folding equilibria are monitored as a function of osmolyte, co-solvent (such as trifluoroethanol, TFE), or denaturant it can be assumed that the equilibrium between unfolded and folded states is linearly dependent on the added solute. This is an assumption of the linear extrapolation method (*4*) which we employ here:

$$\Delta G_{\%TFEv/v} = m \times (\%TFE\ v/v) + \Delta G_0 \quad \text{Eq. 7}$$

Where $\Delta G_{\%TFEv/v}$ is the free energy of the folded-unfolded equilibrium at some specified volume percentage of TFE, m is the proportionality constant by which the folding equilibrium free energy changes with addition of TFE, and ΔG_0 is the equilibrium folding free energy in the absence of any TFE. In the case of circular dichroism measurements, there is a change in absorption of circularly polarized light with a change in structure. This signal change, when plotted as a function of % TFE v/v, creates a sigmoidal transition from which the fraction of unfolded species (f_U) can be represented:

$$f_U = ([\theta]_{\%TFEv/v} - [\theta]_{min})/([\theta]_{max} - [\theta]_{min}) \quad \text{Eq. 8}$$

Where $[\theta]_{\%TFEv/v}$ is the absorption of circularly polarized at different volume percentages of TFE, $[\theta]_{min}$ is the absorption in the absence of TFE where there is no folded structure, and $[\theta]_{max}$ is the absorption where there is constant helical structure with addition of TFE. By calculating f_U at all volume percentages of TFE, equilibrium constants ($K_{eq,\ \%TFE}$) and folding free energies ($\Delta G_{\%TFEv/v}$) can be calculated for each data point:

$$K_{eq,\ \%TFE} = f_U/(1-f_U) \quad \text{Eq. 9}$$
$$\Delta G_{\%TFEv/v} = -RT\ln(K_{eq,\ \%TFE}) \quad \text{Eq. 10}$$

A plot of $\Delta G_{\%TFEv/v}$ from Eq. 10 versus % TFE v/v will yield a linear correlation upon which linear regression analysis can be performed to obtain the slope (m) and intercept (ΔG_0) of Eq. 7 above.

While the above approach provides the desired value for the folded-unfolded equilibrium in the absence of TFE, we further analyzed the data with a non-linear least squares regression fitting of the raw data so that we could simultaneously fit two wavelengths reporting on the

transition (198 nm and 222 nm) to a single set of m-values and ΔG_0. The signal measured by circular dichroism is dependent on the fraction of unfolded protein. To model the folding transition, we use the following expression to describe the experimental data:

$$[\theta]_{fit} = f_U \times ([\theta]_F - [\theta]_U) + [\theta]_U \qquad \text{Eq. 11}$$

Where $[\theta]_{fit}$ is the modeled signal, $[\theta]_F$ is the absorption for maximally folded protein, and $[\theta]_U$ is the absorption for unfolded protein. In the non-linear least squares regression fitting, both $[\theta]_F$ and $[\theta]_U$ are fit parameters. However, absorption values taken directly from the raw data both in the absence of TFE (for $[\theta]_U$) and when there is no additional gain of folded structure upon addition of TFE (for $[\theta]_F$) can be used as close starting values. These parameters did not change substantially during the fitting process (Table 1). Since f_U is directly related to the folded-unfolded equilibrium constant (Eq. 9) and the equilibrium constant is related to free energy in the presence of TFE (Eq. 10) which in turn is linearly related to % TFE v/v (Eq. 7), then simple rearrangement and substitution of equations will give a modified expression for $[\theta]_{fit}$ in terms of the four fit parameters used for non-linear regression:

$$[\theta]_{fit} = ((e^{-(m*(\%TFEv/v)+\Delta G0)/(RT)})/(e^{-(m*(\%TFEv/v)+\Delta G0)/(RT)} + 1)) \times ([\theta]_F - [\theta]_U) + [\theta]_U \qquad \text{Eq. 12}$$

With Eq. 12 used to calculate the theoretical absorption of circularly polarized light as a function of % TFE v/v, we used the solver function of Excel to minimize the sum of the square differences between experimental and calculated fit values by manipulating the four parameters of m, ΔG_0, $[\theta]_F$ and $[\theta]_U$ in a manner similar to that described previously.(*5*, *6*) In addition to using absorption values from the raw data for $[\theta]_F$ and $[\theta]_U$ as described above, we also used m and ΔG_0 parameters obtained from the initial linear regression analysis of the linear-extrapolation method. Using these four starting parameters in Eq. 12 already does a reasonable job of describing the data. However, application of solver for further error minimization improves the total sum of the square differences between raw and fit values. After fitting the raw data sets, both the data and fit were normalized for side-by-side comparison in the main text.

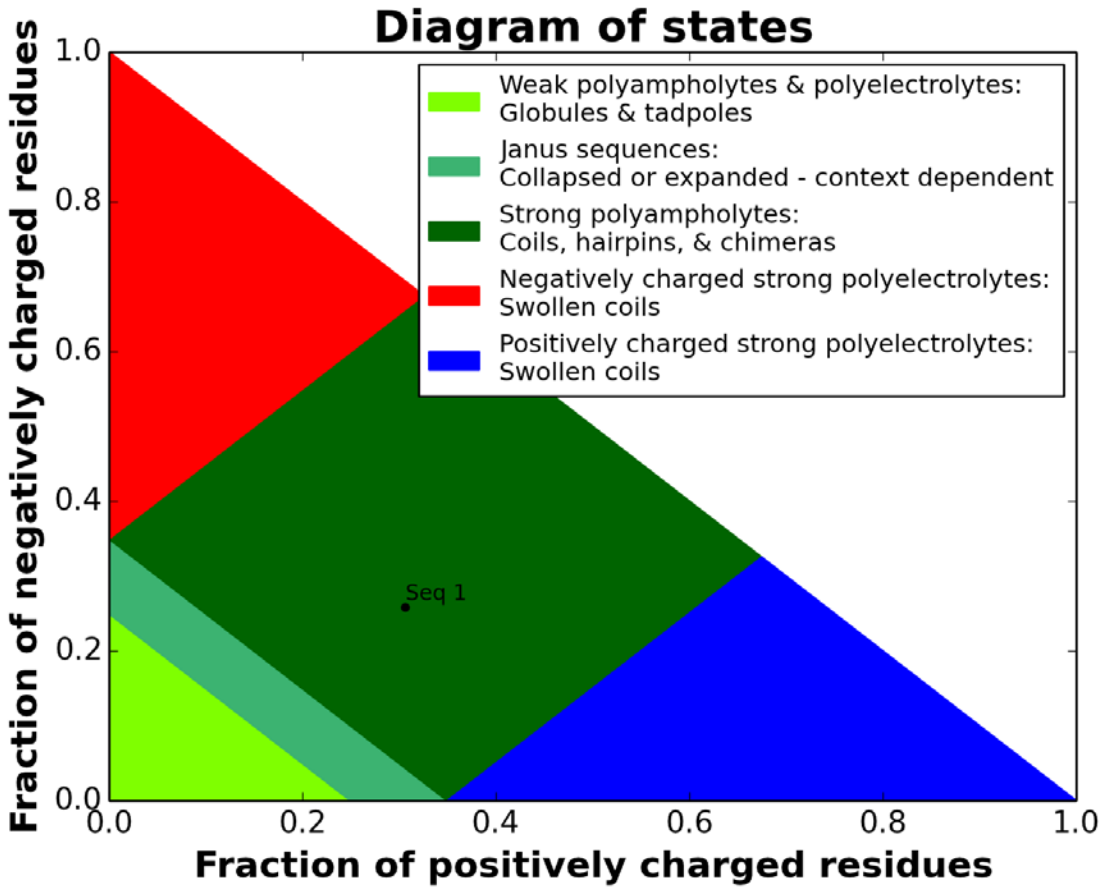

Supporting Figure 1. Position of Syt 1 IDR in sequence charge-dependent phase diagram of structural states. Note that location of the Syt 1 IDR, indicated by Seq 1 data point, suggests it likely samples coil and/or hairpin-like structural states in an environment whose dielectric constant is similar to water.

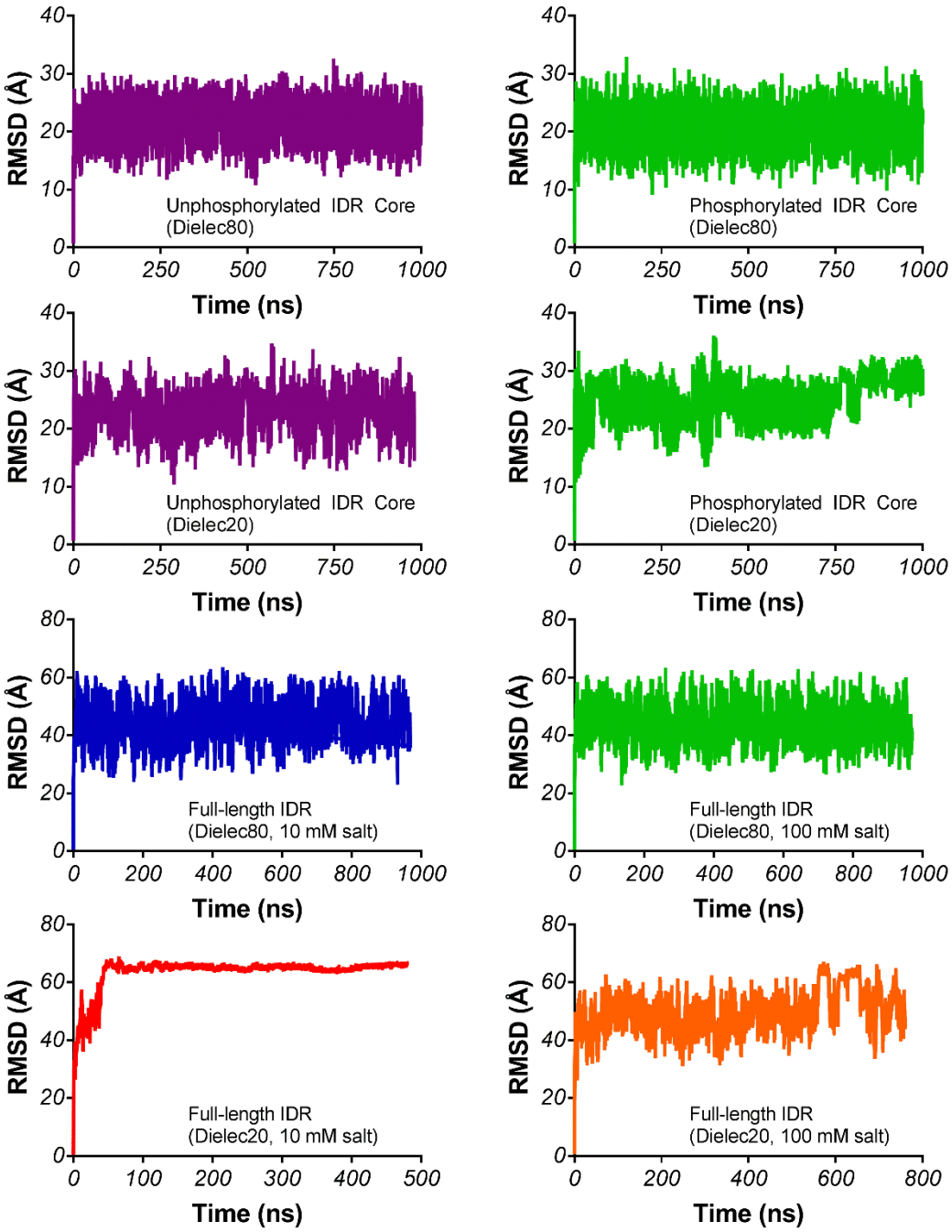

Supporting Figure 2. RMSD of Syt 1 IDR constructs used in MD simulations. Core region peptides (residues 97-129) in unphosphorylated (purple) and phosphorylated (green) states and at dielectric constants of both ε=80 and ε=20 are shown in top four panels. The full-length peptides (residues 80-141) at dielectric constant and salt concentration of ε=80 and 10 mM (blue), ε=80 and 100 mM (green), ε=20 and 10 mM (red), ε=20 and 100 mM (orange) are shown in the bottom four panels. Note that each peptide reaches equilibrium rapidly.

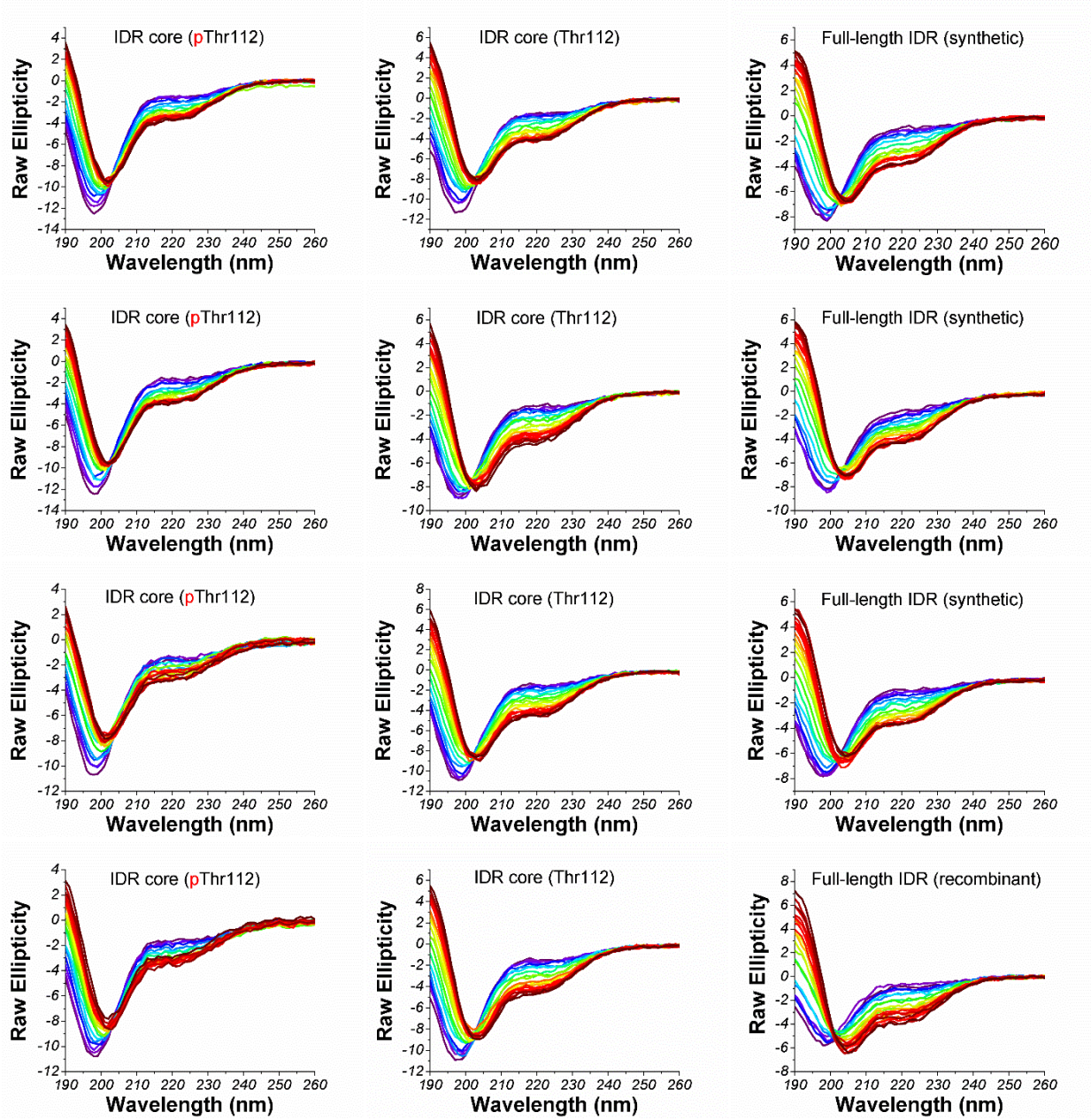

Supporting Figure 3. TFE-induced folding of Syt1 IDR. The left column shows partial folding of the IDR core residues (97-130) with Thr112 phosphorylated. Note its restricted transition. The middle column shows partial folding of IDR core residues (97-130) with Thr112 in its unphosphorylated state. The right column shows partial folding of the full length IDR (residues 80-140). Note that the top three panels in this column are replicates of the synthesized peptide and the bottom panel is the recombinantly expressed IDR that includes a C-terminal his-tag. Violet to red corresponds to a 0-60% v/v TFE range in increments of 3%.

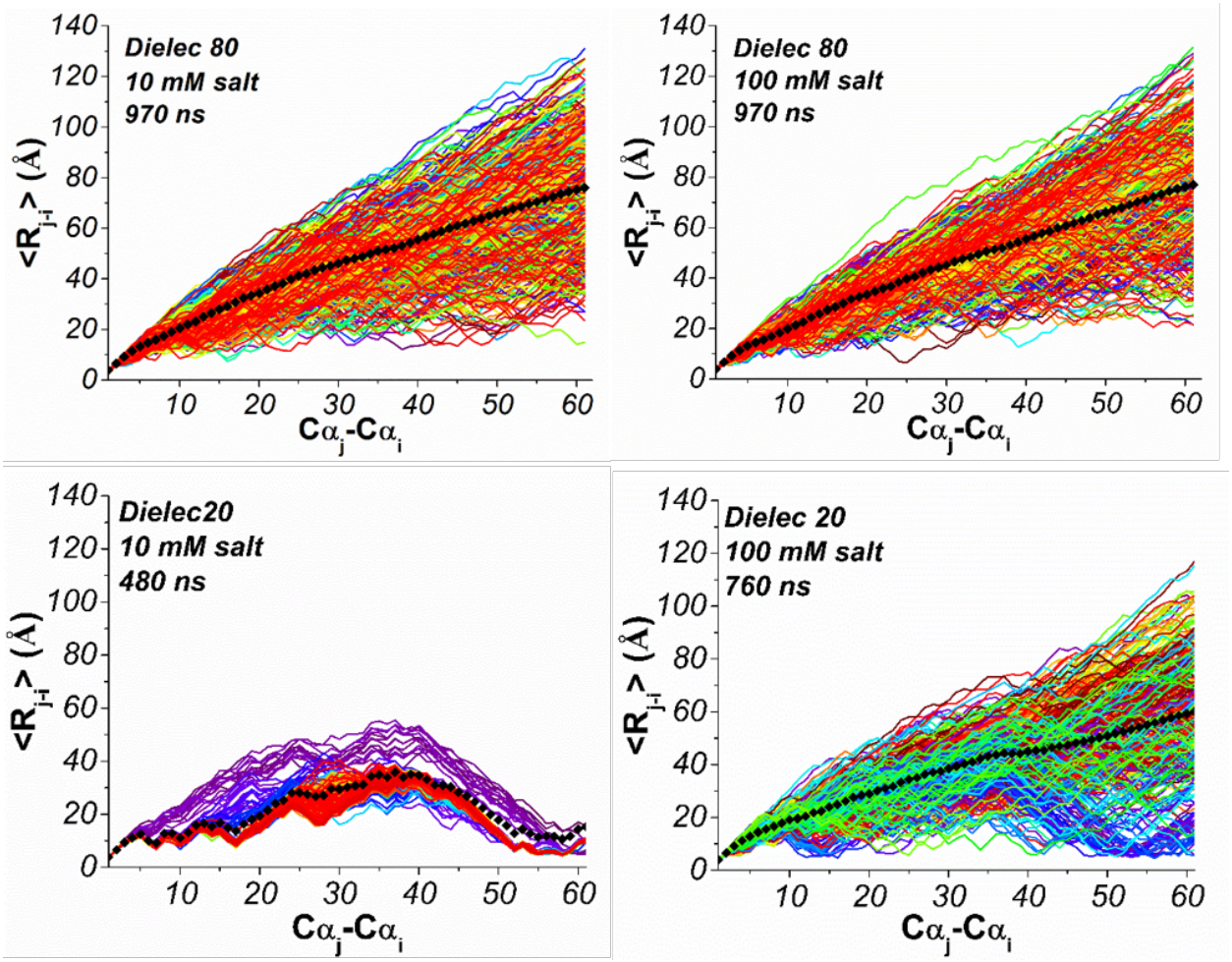

Supporting Figure 4. Simulated inter-residue distances of full-length Syt 1 IDR under varied dielectric constant and salt conditions during the course of each trajectory. Black diamonds indicate the average structure.

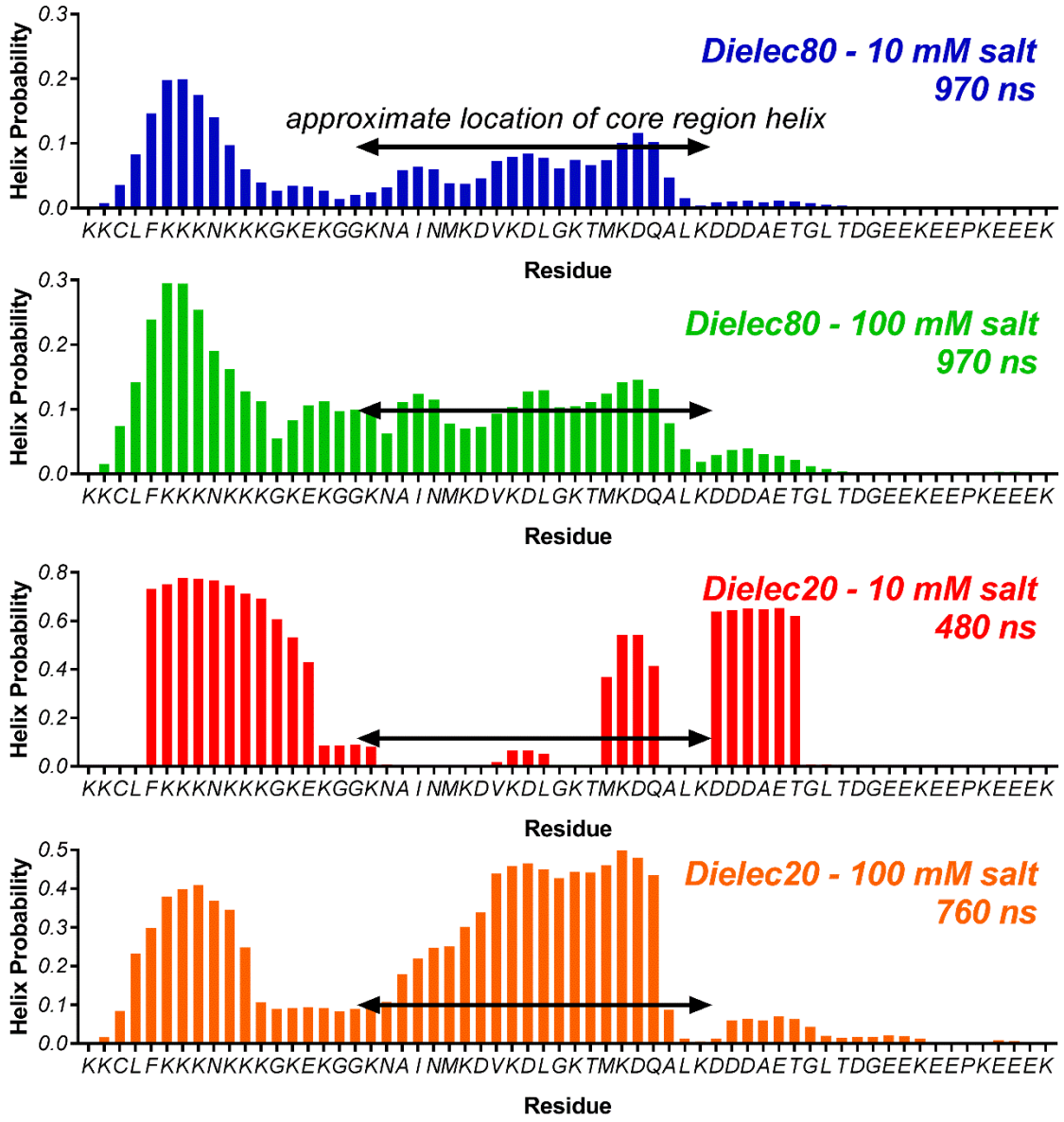

Supporting Figure 5. Helix probability histograms (determined as described in main text) for full-length Syt 1 IDR sequence. Black arrows for all four histograms indicate approximate core residue region. In all cases, arrows align with 0.1 on the probability axis to aid comparison. Also noteworthy is that, under all four conditions, helical content in the acidic C-terminus was markedly low.

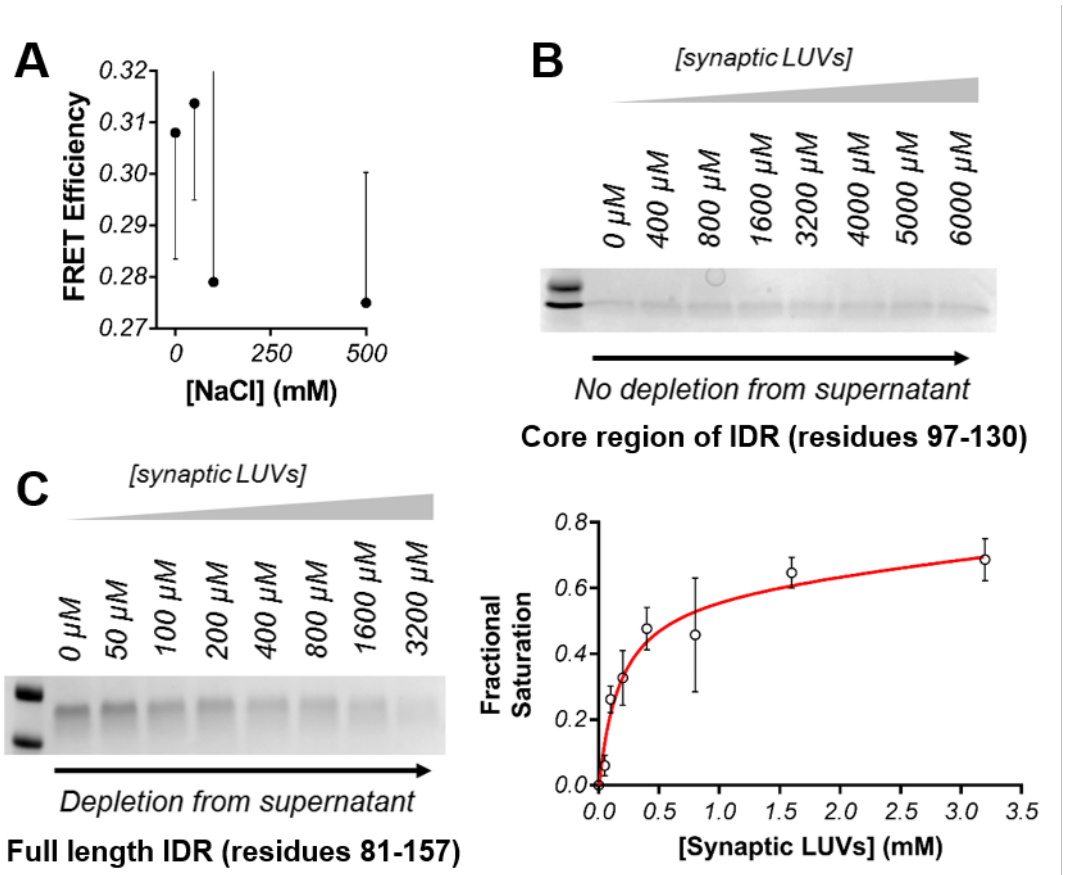

Supporting Figure 6. Potential factors influencing full-length IDR compaction. (A) FRET efficiency was not significantly affected by salt. (B) Core region Syt 1 IDR (representative of n=2) as a synthetic peptide in a co-sedimentation assay with synaptic vesicle mimic LUVs. (C) Full-length Syt 1 IDR (left, representative of n=3) as a synthetic peptide in a co-sedimentation assay with synaptic vesicle mimic LUVs and (right) the resultant binding curve (K_D = 169±82 µM). Collectively, the presence of either peptide in the supernatant indicates that the peptide containing the polybasic N-terminus is binding competent. This suggests that the basic N-terminus, in addition to transiently interacting with the negative C-terminus of the IDR sequence, also interacts with acidic lipids in a synaptic vesicle membrane and likely has two competing interactions (lipid – intermolecular; negative C-terminus – intramolecular) that could influence propensity to exist in compact structural state.

Supporting Table 1. Calculated kappa for blob g=5.

For g = 5										
i	**+**	**-**	$\mathbf{f_+}$	$\mathbf{f_-}$	$\boldsymbol{\sigma_i}$	$\boldsymbol{(\sigma_i - \sigma)^2}$	$\boldsymbol{\sum N_{blob}}$	**# of blobs**	**δ**	$\boldsymbol{\kappa_{g=5}}$
1	2	0	0.4	0	0.400	0.157	6.927	58	0.119	0.238
2	2	0	0.4	0	0.400	0.157				
3	2	0	0.4	0	0.400	0.157				
4	3	0	0.6	0	0.600	0.355				
5	3	0	0.6	0	0.600	0.355				
6	4	0	0.8	0	0.800	0.633				
7	4	0	0.8	0	0.800	0.633				
8	4	0	0.8	0	0.800	0.633				
9	3	0	0.6	0	0.600	0.355				
10	4	0	0.8	0	0.800	0.633				
11	3	1	0.6	0.2	0.200	0.038				
12	3	1	0.6	0.2	0.200	0.038				
13	2	1	0.4	0.2	0.067	0.004				
14	2	1	0.4	0.2	0.067	0.004				
15	2	1	0.4	0.2	0.067	0.004				
16	2	0	0.4	0	0.400	0.157				
17	1	0	0.2	0	0.200	0.038				
18	1	0	0.2	0	0.200	0.038				
19	1	0	0.2	0	0.200	0.038				
20	0	0	0	0						
21	1	0	0.2	0	0.200	0.038				
22	1	1	0.2	0.2	0.000	0.000				
23	1	1	0.2	0.2	0.000	0.000				
24	2	1	0.4	0.2	0.067	0.004				
25	2	2	0.4	0.4	0.000	0.000				
26	1	2	0.2	0.4	0.067	0.004				
27	1	1	0.2	0.2	0.000	0.000				
28	2	1	0.4	0.2	0.067	0.004				
29	1	1	0.2	0.2	0.000	0.000				
30	1	0	0.2	0	0.200	0.038				
31	2	0	0.4	0	0.400	0.157				
32	2	1	0.4	0.2	0.067	0.004				
33	1	1	0.2	0.2	0.000	0.000				
34	1	1	0.2	0.2	0.000	0.000				
35	1	1	0.2	0.2	0.000	0.000				
36	1	1	0.2	0.2	0.000	0.000				
37	1	1	0.2	0.2	0.000	0.000				
38	1	2	0.2	0.4	0.067	0.004				
39	1	3	0.2	0.6	0.200	0.038				
40	1	3	0.2	0.6	0.200	0.038				
41	0	4	0	0.8	0.800	0.633				
42	0	3	0	0.6	0.600	0.355				
43	0	2	0	0.4	0.400	0.157				
44	0	1	0	0.2	0.200	0.038				
45	0	1	0	0.2	0.200	0.038				
46	0	1	0	0.2	0.200	0.038				
47	0	1	0	0.2	0.200	0.038				
48	0	2	0	0.4	0.400	0.157				
49	0	3	0	0.6	0.600	0.355				

50	1	3	0.2	0.6	0.200	0.038	
51	1	3	0.2	0.6	0.200	0.038	
52	1	4	0.2	0.8	0.360	0.127	
53	1	3	0.2	0.6	0.200	0.038	
54	2	2	0.4	0.4	0.000	0.000	
55	1	3	0.2	0.6	0.200	0.038	
56	1	3	0.2	0.6	0.200	0.038	
57	1	3	0.2	0.6	0.200	0.038	
58	2	3	0.4	0.6	0.040	0.001	

Supporting Table 2. Calculated kappa for g=6.

for g=6										
i	+	-	f_+	f_-	σ_i	$(\sigma_i - \sigma)^2$	$\sum N_{blob}$	# of blobs	δ	$\kappa_{g=6}$
1	3	0	0.500	0.000	0.500	0.246	6.170	57	0.108	0.215
2	3	0	0.500	0.000	0.500	0.246				
3	3	0	0.500	0.000	0.500	0.246				
4	3	0	0.500	0.000	0.500	0.246				
5	4	0	0.667	0.000	0.667	0.439				
6	5	0	0.833	0.000	0.833	0.688				
7	5	0	0.833	0.000	0.833	0.688				
8	4	0	0.667	0.000	0.667	0.439				
9	4	0	0.667	0.000	0.667	0.439				
10	4	1	0.667	0.167	0.300	0.088				
11	4	1	0.667	0.167	0.300	0.088				
12	3	1	0.500	0.167	0.167	0.026				
13	2	1	0.333	0.167	0.056	0.003				
14	3	1	0.500	0.167	0.167	0.026				
15	2	1	0.333	0.167	0.056	0.003				
16	2	0	0.333	0.000	0.333	0.108				
17	1	0	0.167	0.000	0.167	0.026				
18	1	0	0.167	0.000	0.167	0.026				
19	1	0	0.167	0.000	0.167	0.026				
20	1	0	0.167	0.000	0.167	0.026				
21	1	1	0.167	0.167	0.000	2.E-05				
22	1	1	0.167	0.167	0.000	2.E-05				
23	2	1	0.333	0.167	0.056	0.003				
24	2	2	0.333	0.333	0.000	2.E-05				
25	2	2	0.333	0.333	0.000	2.E-05				
26	1	2	0.167	0.333	0.056	0.003				
27	2	1	0.333	0.167	0.056	0.003				
28	2	1	0.333	0.167	0.056	0.003				
29	1	1	0.167	0.167	0.000	2.E-05				
30	2	0	0.333	0.000	0.333	0.108				
31	2	1	0.333	0.167	0.056	0.003				
32	2	1	0.333	0.167	0.056	0.003				
33	1	1	0.167	0.167	0.000	2.E-05				
34	1	1	0.167	0.167	0.000	2.E-05				
35	2	1	0.333	0.167	0.056	0.003				
36	1	2	0.167	0.333	0.056	0.003				
37	1	2	0.167	0.333	0.056	0.003				
38	1	3	0.167	0.500	0.167	0.026				
39	1	3	0.167	0.500	0.167	0.026				
40	1	4	0.167	0.667	0.300	0.088				
41	0	4	0.000	0.667	0.667	0.439				
42	0	3	0.000	0.500	0.500	0.246				
43	0	2	0.000	0.333	0.333	0.108				
44	0	1	0.000	0.167	0.167	0.026				
45	0	2	0.000	0.333	0.333	0.108				
46	0	1	0.000	0.167	0.167	0.026				
47	0	2	0.000	0.333	0.333	0.108				
48	0	3	0.000	0.500	0.500	0.246				
49	1	3	0.167	0.500	0.167	0.026				

50	1	4	0.167	0.667	0.300	0.088	
51	1	4	0.167	0.667	0.300	0.088	
52	1	4	0.167	0.667	0.300	0.088	
53	2	3	0.333	0.500	0.033	0.001	
54	2	3	0.333	0.500	0.033	0.001	
55	1	4	0.167	0.667	0.300	0.088	
56	1	4	0.167	0.667	0.300	0.088	
57	2	3	0.333	0.500	0.033	0.001	

Supporting Table 3. MD-derived secondary structure for Syt 1 IDR core region. Turn (T), β-sheet (B), helix (H) and coil (C) are shown as fractions for each residue.

	Unphosphorylated Dielec80				Unphosphorylated Dielec20				Phosphorylated Dielec80				Phosphorylated Dielec20			
Res	T	B	H	C	T	B	H	C	T	B	H	C	T	B	H	C
97	0.120	0.000	0.000	0.880	0.104	0.000	0.000	0.896	0.126	0.000	0.000	0.874	0.270	0.000	0.000	0.730
98	0.229	0.000	0.005	0.766	0.208	0.027	0.008	0.751	0.244	0.002	0.003	0.750	0.320	0.001	0.003	0.676
99	0.359	0.000	0.020	0.621	0.380	0.027	0.040	0.505	0.379	0.002	0.014	0.605	0.652	0.002	0.006	0.340
100	0.457	0.000	0.083	0.460	0.547	0.000	0.144	0.305	0.500	0.000	0.064	0.435	0.676	0.084	0.039	0.202
101	0.442	0.000	0.097	0.460	0.551	0.000	0.173	0.277	0.484	0.000	0.077	0.438	0.686	0.099	0.045	0.169
102	0.443	0.000	0.104	0.454	0.540	0.000	0.194	0.265	0.486	0.000	0.078	0.436	0.711	0.089	0.064	0.135
103	0.519	0.000	0.092	0.389	0.559	0.000	0.185	0.253	0.550	0.000	0.045	0.405	0.614	0.118	0.061	0.208
104	0.445	0.000	0.093	0.462	0.404	0.024	0.179	0.348	0.474	0.002	0.030	0.494	0.682	0.107	0.052	0.159
105	0.394	0.000	0.089	0.517	0.355	0.024	0.194	0.419	0.448	0.002	0.035	0.515	0.604	0.000	0.048	0.348
106	0.418	0.000	0.128	0.454	0.361	0.000	0.307	0.331	0.482	0.000	0.059	0.459	0.664	0.084	0.034	0.218
107	0.352	0.000	0.153	0.495	0.355	0.000	0.335	0.310	0.440	0.000	0.073	0.487	0.612	0.094	0.181	0.113
108	0.342	0.000	0.158	0.499	0.412	0.000	0.327	0.261	0.414	0.000	0.065	0.522	0.228	0.193	0.170	0.409
109	0.354	0.000	0.149	0.497	0.373	0.000	0.336	0.287	0.359	0.000	0.044	0.597	0.234	0.115	0.174	0.478
110	0.486	0.000	0.102	0.412	0.458	0.000	0.287	0.252	0.331	0.000	0.009	0.660	0.220	0.000	0.000	0.780
111	0.448	0.001	0.141	0.411	0.445	0.006	0.295	0.253	0.193	0.000	0.007	0.799	0.087	0.000	0.033	0.879
112	0.448	0.001	0.147	0.404	0.422	0.010	0.285	0.282	0.160	0.000	0.010	0.830	0.502	0.000	0.123	0.374
113	0.520	0.000	0.162	0.317	0.485	0.011	0.288	0.215	0.324	0.000	0.026	0.650	0.612	0.000	0.221	0.167
114	0.527	0.000	0.203	0.270	0.484	0.010	0.323	0.182	0.462	0.000	0.057	0.482	0.621	0.000	0.343	0.035
115	0.520	0.000	0.226	0.255	0.531	0.000	0.324	0.146	0.492	0.000	0.086	0.421	0.578	0.000	0.398	0.024
116	0.525	0.001	0.205	0.269	0.516	0.000	0.295	0.190	0.522	0.000	0.083	0.395	0.591	0.000	0.350	0.059
117	0.482	0.001	0.122	0.395	0.501	0.011	0.124	0.362	0.484	0.000	0.053	0.464	0.623	0.000	0.120	0.258
118	0.380	0.000	0.058	0.562	0.388	0.015	0.060	0.534	0.384	0.000	0.022	0.593	0.393	0.000	0.018	0.589
119	0.284	0.000	0.019	0.697	0.309	0.013	0.024	0.652	0.296	0.000	0.008	0.696	0.243	0.000	0.007	0.750
120	0.228	0.000	0.022	0.750	0.257	0.005	0.052	0.685	0.242	0.000	0.011	0.747	0.330	0.000	0.013	0.658
121	0.190	0.000	0.024	0.787	0.237	0.000	0.070	0.693	0.211	0.000	0.017	0.773	0.305	0.000	0.067	0.628
122	0.220	0.000	0.026	0.754	0.268	0.000	0.073	0.659	0.237	0.000	0.019	0.744	0.349	0.000	0.084	0.567
123	0.335	0.000	0.023	0.642	0.363	0.000	0.061	0.574	0.333	0.000	0.016	0.650	0.446	0.005	0.091	0.459
124	0.309	0.000	0.019	0.672	0.350	0.000	0.056	0.593	0.312	0.000	0.016	0.672	0.467	0.006	0.079	0.449
125	0.308	0.000	0.016	0.676	0.338	0.001	0.040	0.620	0.312	0.000	0.013	0.676	0.420	0.003	0.060	0.518
126	0.260	0.000	0.009	0.731	0.288	0.000	0.018	0.691	0.255	0.000	0.006	0.739	0.349	0.000	0.021	0.630
127	0.122	0.000	0.004	0.875	0.146	0.000	0.008	0.845	0.126	0.000	0.002	0.872	0.150	0.000	0.005	0.846
128	0.057	0.000	0.000	0.943	0.067	0.000	0.000	0.932	0.053	0.000	0.000	0.947	0.065	0.000	0.000	0.935
129	0.001	0.000	0.000	0.999	0.001	0.000	0.000	0.999	0.001	0.000	0.000	0.999	0.001	0.000	0.000	0.999

Supporting References

1. Das, R. K., and Pappu, R. V. (2013) Conformations of intrinsically disordered proteins are influenced by linear sequence distributions of oppositely charged residues, *Proc Natl Acad Sci U S A 110*, 13392-13397.
2. Fealey, M. E., Mahling, R., Rice, A. M., Dunleavy, K., Kobany, S. E., Lohese, K. J., Horn, B., and Hinderliter, A. (2016) Synaptotagmin I's Intrinsically Disordered Region Interacts with Synaptic Vesicle Lipids and Exerts Allosteric Control over C2A, *Biochemistry 55*, 2914-2926.
3. Rice, A. M., Mahling, R., Fealey, M. E., Rannikko, A., Dunleavy, K., Hendrickson, T., Lohese, K. J., Kruggel, S., Heiling, H., Harren, D., Sutton, R. B., Pastor, J., and Hinderliter, A. (2014) Randomly organized lipids and marginally stable proteins: a coupling of weak interactions to optimize membrane signaling, *Biochim Biophys Acta 1838*, 2331-2340.
4. Santoro, M. M., and Bolen, D. W. (1988) Unfolding free energy changes determined by the linear extrapolation method. 1. Unfolding of phenylmethanesulfonyl alpha-chymotrypsin using different denaturants, *Biochemistry 27*, 8063-8068.
5. Fealey, M. E., Gauer, J. W., Kempka, S. C., Miller, K., Nayak, K., Sutton, R. B., and Hinderliter, A. (2012) Negative coupling as a mechanism for signal propagation between C2 domains of synaptotagmin I, *PLoS One 7*, e46748.
6. Gauer, J. W., Sisk, R., Murphy, J. R., Jacobson, H., Sutton, R. B., Gillispie, G. D., and Hinderliter, A. (2012) Mechanism for calcium ion sensing by the C2A domain of synaptotagmin I, *Biophys J 103*, 238-246.